Journal of Electroceramics 5:2, 93–110, 2000

Analytical Functions for the dc and ac Conductivity of Conductor-Insulator Composites

DAVID S McLACHLAN

Physics Department and Condensed Matter Research Unit, University of the Witwatersrand, Johannesburg 2050
E-mail: mclachlan@physnet.phys.wits.ac.za

Submitted February 13, 1999; Revised May 5, 1999; Accepted May 5, 1999

Abstract. The Maxwell-Wagner and the Bruggeman Symmetric and Asymmetric Media equations are introduced and the well defined microstructures for which these effective media equations apply are emphasized.

The microstructures characterising percolation systems and the resultant critical volume fractions are then discussed. After this the concept of scaling, the percolation expressions and a new two exponent analytical phenomenological equation are introduced and their interrelationship is examined.

The information obtainable from dc measurements is investigated and then simulations of impedance and modular spectra obtained from the effective media equations are given and the implications of these results discussed. Followed this, results for the complex ac conductivity of a nearly ideal continuum systems are given and it is shown that the conductivity above and the dielectric term below the critical volume fraction can be scaled onto analytical curves, using parameters obtained from dc conductivity measurements. Lastly simulations of the type of impedance spectra and dispersion relations that might be observed for systems with a percolation microstructure but non ideal insulating and conducting components are given and discussed.

Keywords: electrical conductivity, effective media theories, percolation, composites, impedence spectroscopy

I. Introduction

Quantitative models, or even semi quantitative ones, for the complex conductivity (dielectric constant) of electroceramics (or composites) can be used to not only understand their properties and hopefully design new or better electroceramics, but can also be used to determine the electrical properties of the components and to gauge the microstructure from electrical measurements of these materials. In this paper we present two classes of models for binary systems, although with some ingenuity, these can often be applied to three or more component systems. The first are the effective media equations, where the only parameters are the conductivities of the components, as the microstructures are well defined. The second are the percolation equations and the related one and two exponent phenomelogical equations, henceforth referred to as the GEM equations, both of which need an additional two or three parameters to characterize the microstructure or distribution and interconnectivity of the components. Unfortunately, one cannot, as yet, use these equations to design and characterize all electroceramics in a quantitative way, but an understanding of these equations, and the microstructures to which they apply, is necessary to understand the conductivity of composite electroceramics, even in a semi quantitative way.

Effective media theories from Maxwell to Maxwell-Wagner (MW) and on to the Bruggeman Symmetric Media (BS) and Asymmetric Media (BA) equations and percolation theories are reviewed, up until 1979, by Landauer [1]. McLachlan [2], also discussed these topics and the one exponent General Effective Media (GEM) equation. Percolation theory is made accessible in the introductory book by

Stauffer and Ahorony [3], a wide range of percolation topics is presented in reference [4] and the electrical properties of inhomogeneous media are reviewed by Bergman and Stroud [5], Nan [6] and Clerc et al. [7].

Emphasis in this article will be placed on isotropic media. For an in depth discussion and derivation of the equations, and more on anisotropic media, the reader is referred to the above review articles [1–7], and the references therein. Due space constraints the author will, where possible, refer to the review articles only. The first section on theory will present the effective media equations and their microstructures, the one thereafter will discuss percolation microstructures and this will be followed by a section on scaling and the percolation equations. These are followed by sections giving experimental results and computer simulations for effective media and percolation systems.

II. Effective Media Theories

The various binary phase effective media, which have a conductivity σ_m (resistivity $\rho_m = 1/\sigma_m$), discussed will all consist of two components, the highly conducting one with a conductivity of σ_h (resistivity $\rho_\ell = 1/\sigma_h$) and a more insulating one characterized by $\sigma_\ell (1/\sigma_\ell = \rho_h)$. In principle, in all equations, one can substitute the appropriate complex dielectric constant $(\varepsilon^* = \varepsilon_r + i\varepsilon_i)$, complex conductivity $(\sigma^* = \sigma_r + i\sigma_i)$ or complex permeability $(\mu^* = \mu_r + i\mu_i)$ for the equivalent σ_m, σ_h or σ_ℓ. The volume fraction of the more conductive component is given by ϕ and the less by $f = 1 - \phi$. Note that in the BS, GEM and percolation equations there are also the ''microstructure'' parameters, ϕ_c (the percolation threshold) and the exponents (s and t).

The first effective media for spherical inclusions equations were due to Maxwell. For dilute dispersions of spheres in a host matrix (valid for f and $\phi \leq 0.1$ [8]), these are

$$\sigma_m(f) = \sigma_h(1 - 3/2f) \tag{1a}$$

$$\rho_m(\phi) = \rho_h(1 - 3\phi). \tag{1b}$$

Equation (1a) is valid when $\sigma_\ell = 0$ and Eq. (1b) when $\rho_\ell = 0$ for the dispersed component. Expressions where $0 < \sigma_\ell < \sigma_h < \infty$ and for anisotropic media, are given in Meredith and Tobias [8]. All valid effective media theories must reduce to these expressions in the dilute limit.

The well known Maxwell-Wagner relationships for spherical inclusions or grains are,

$$\frac{\sigma_m - \sigma_h}{\sigma_m + 2\sigma_h} = f\,\frac{\sigma_\ell - \sigma_h}{\sigma_\ell + 2\sigma_h} \tag{2a}$$

$$\frac{\sigma_m - \sigma_\ell}{\sigma_m + 2\sigma_\ell} = \phi\,\frac{\sigma_h - \sigma_\ell}{\sigma_h + 2\sigma_\ell} \tag{2b}$$

The expressions are often written in terms of ε_m, ε_ℓ and ε_h and called the Claussius-Mossetti relationships. The MW media can be visualized as built up out of a space-filling array of coated spheres, as illustrated in Fig. 1b(i) for Eq. (2a) and Fig. 1b(ii) for Eq. (2b). The coating component forms the host or matrix component (σ_h in Eq. 2a and σ_ℓ in Eq. (2b)) therefore, as the coatings on the spheres persist until f or $\phi = 1$, there is no percolation threshold ($\phi = 0$ or 1 is not a percolation threshold, as the medium then consists of a single component). The Maxwell-Wagner equations are equivalent to the Hashin-Shtrikman (HS) [2,5] upper and lower bounds for the conductivity (resistivity) of an isotropic two component mixture. The microstructures described by the MW and HS equations are also the same. These equations are plotted in curves a and e in Fig. 2.

Bruggeman asymmetric media equations, for spherical inclusions or grains, are [1,8],

$$\frac{(\sigma_m - \sigma_\ell)^3}{\sigma_m} = (1 - f)\,\frac{^3(\sigma_h - \sigma_\ell)^3}{\sigma_h} \tag{3a}$$

$$\frac{(\sigma_m - \sigma_h)^3}{\sigma_m} = (1 - \phi)\,\frac{^3(\sigma_\ell - \sigma_h)^3}{\sigma_\ell} \tag{3b}$$

The building ''blocks'' for the media described by Eq. (3a) are illustrated in column c(i) of Fig. 1 and for Eq. (3b) in column c(ii). Again this requires a very large range of the building block or sphere sizes and a specific host or matrix component and there is no percolation threshold. Equations (3a) and (b) are plotted in Fig. 2 as b and d and are derived in Landauer [1] and [8]. Ellipsoidal grains or building blocks are discussed in Meredith and Tobias [8].

Bruggeman's symmetric media equation (BS) for an isotropic media, which is built up out of a very large range of the conducting and insulating spheres, as shown in column a of Fig. 1, is

$$\phi(\sigma_h - \sigma_m)/(\sigma_h + A\sigma_m) + (1 - \phi)$$
$$(\sigma_\ell - \sigma_m)/(\sigma_\ell + A\sigma_m) = 0 \tag{4}$$

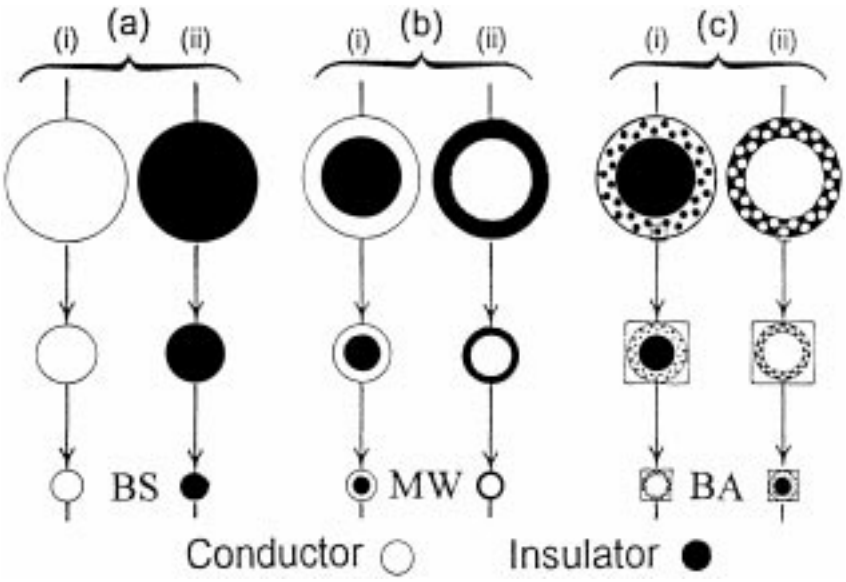

Fig. 1. This figure illustrates the building blocks for the microstructures which are characterized by (a. i and ii) the Bruggeman's Symmetric Media Equation (Eq. (4)), (b. i and ii) the Maxwell-Wagner equation (Eqs. (2a) and (b)) and (c. i and ii) Bruggeman's Asymmetric Media equations (Eqs. (3a) and (b)). Note that these media require a very large range in the size of the spheres and that spheres of similar size be well separated.

A depends on the demagnetization coefficient of the ellipsoids building up the media [8] and is 2 for spheres. The randomly arranged space-filling spheres, shown in columns a(i) and a(ii) of Fig. 1, are randomly assigned to be conducting or non-conducting, so that a fraction ϕ of them have the higher conductivity (therefore $1-\phi$ or f of the spheres have the lower conductivity). Reference [8], and the references therein, give alternate expression for A. In general A is determined by the demagnetization coefficients of the ellipsoids making up the media and gives ϕ_c, as A can always be written as $(1-\phi_c)/\phi_c$, even when the media are made up out of oriented or randomly oriented ellipsoids. Equation (4) is plotted as curve c in Fig. 2.

Equations (2a) and (3a) reduce to Eq. (1a) when f is small and $\sigma_\ell = 0$. Equations (2b) and (3b) reduce to Eq. (1b) when ϕ is small and $\sigma_h = \infty$ or $\rho_\ell = 0$, the equations being rewritten in terms of ρ_m, ρ_ℓ and ρ_h to avoid the infinities. However, Eq. (4) reduces to Eq. (1a) for all $f(1-\phi)$ if $\sigma_\ell = 0$ and to Eq. (1b), for all ϕ when Eq. (4) is rewritten in terms of ρ_m, ρ_ℓ and ρ_h with $\sigma_h = \infty$ or $\rho_\ell = 0$. Therefore Eq. (4) predicts a metal-insulator $(\sigma_m = 0)$ transition (MIT) when $f = f_c = 2/3(\phi = 1/3)$ and $\sigma_\ell = 0$ and a perfect conductor-normal $(\rho_m = 0)$ transition (PNT) when $\phi = \phi_c = 1/3$. This behavior of $\sigma_m(\rho_m)$ is also observed at an ideal percolation threshold. Therefore, the microstructure characterized by the BS theory leads to a percolation type behavior. Equation (4) is plotted as curve c in Fig. 2 for $A = 2(\phi_c = 1/3)$.

Figure 2 shows that the resistivity of media described by Eqs. (2a) and (2e) and Eqs. (3b) and (3d) is dominated by the host or matrix material until f or ϕ approaches 1. However, if there is a percolation type transition, as illustrated by Eq. (4) (curve c in Fig. 2), the properties of the medium rapidly change from being dominated by one component to the other near ϕ_c (or f_c), where $0 < \phi_c, f_c < 1$.

An effective medium is one in which each sphere (ellipsoid) is surrounded by a mixture of the two components that has the mean or effective value for the medium. This requires that the spheres (ellipsoids) have an effectively infinite range in size, and that the larger spheres are separated by material containing smaller spheres. The more usual type of percolation system, where spheres (ellipsoids, grains) of similar size come, or nearly come into contact with each other are not effective media. In practice effective media theories work best for lower values of f or ϕ, where the spheres (ellipsoids) are further apart.

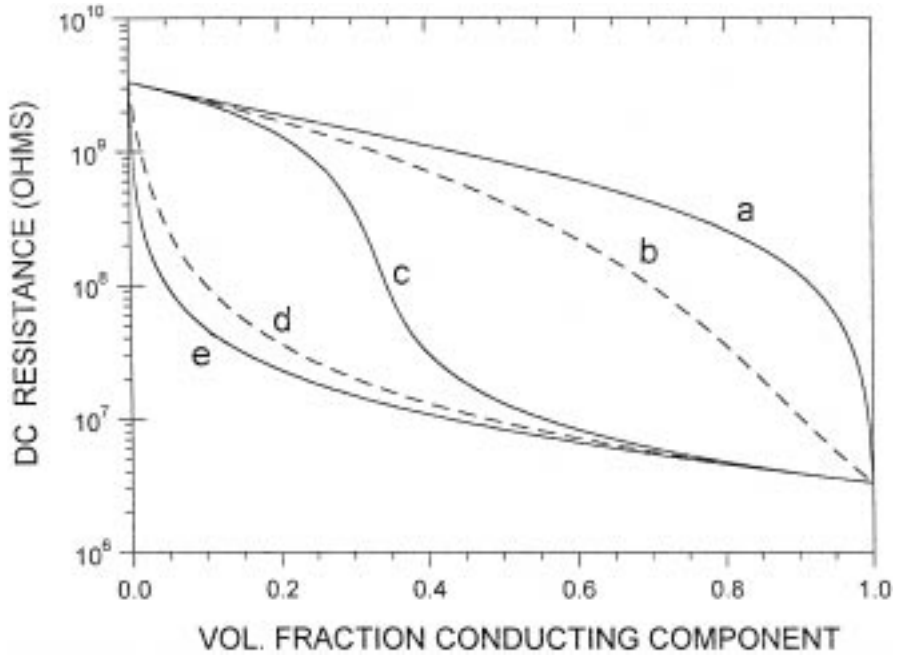

Fig. 2. Resistivity bounds for a two component media as a function of volume fraction. One component has a resistivity $\rho_h = 3.33 \times 10^9\ \Omega\,\mathrm{m}$ ($\sigma_\ell = 3 \times 10^{-8}$) and the other $\rho_\ell = 3.33 \times 10^6\ \Omega\ \mathrm{m}$ ($\sigma_h = 3 \times 10^{-5}$). The curves are the Maxwell-Wagner equations (Eqs. (3a) and (b)) or the Hashin-Shtrikman upper and lower bounds (a) and (e), the Bruggeman Asymetric Eqs. (Eqs. (4a) and (b)) (b) and (d), and the Bruggeman Symmetric Equation (Eq. (5)) (c).

III. The Critical Volume Fraction in Percolation Systems

The percolation equations are obeyed by computer simulations where conducting bonds and sites (connected to all nearest neighbors) are placed at random on a 2 or 3 dimensional Bravais lattice [2,5,6,9]. The fraction of occupied bonds or sites necessary to produce a conducting path through all lattice types is well known [2,9]. If conducting spheres, of just sufficient size to touch their nearest neighbors, are placed at random on the sites of a 3d lattice, it is found that at the percolation threshold the volume fraction, occupied by the spheres, ϕ_c is at 0.16 ± 0.02 [2,9]. If metal ball bearings and glass beads of equal size are placed in a large container it is found that at ϕ_c the volume fraction of the ball bearings is also close to 0.16 [2,9]. In continuum (two component) percolation theory, a ϕ_c close to 0.16 is now taken to characterize a random media, but other values of ϕ_c are also permitted.

In both lattice and continuum cases, the theory predicts that just below the percolation threshold the bonds, sites or conducting grains lie mainly in large clusters with mean diameters $\xi \approx a_o/|\phi - \phi_c|^{\nu}$. At $|\phi - \phi_c| = 0$ the largest cluster becomes infinite and leads to a dc conduction or percolation path through the sample. Here ξ is the coherence length, a_o is the mean grain size, and ν a critical index 0.85 in 3d [3,5,9].

For ϕ_c less than 0.16, two models can be considered. The first is the grain consolidation model [2] illustrated in Fig. 6 of McLachlan [10] and Fig. 3 of Roberts and Schwartz [11]. The starting two phase composite and the conducting two phase composites, remaining after the pure insulating phase has started to grow (from out of the above two phase composites), is treated as a single composite phase (black in Fig. 3). The second phase is the monophase insulating ''spheres'' (white in Fig. 3). The model for ϕ_c starts with the nucleation of a random array of small insulating spheres embedded in the two phase composite (Fig. 3a). The insulating spheres then grow to form a random-close packed lattice with point contacts on the surfaces (Fig. 3b). As the radii of the insulating spheres increase further, the

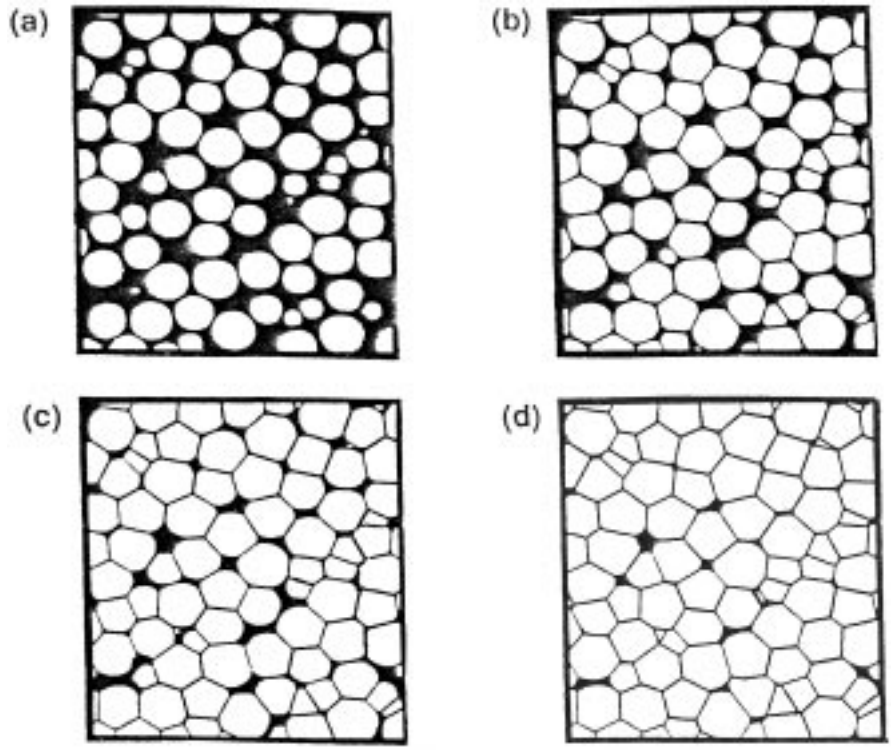

Fig. 3. Computer-synthesized cross sections of a sample of material produced by consolidating a distribution of spherical grains. The thin straight lines along the grain-to-grain contacts have been included for clarity. The illustrated stages are (a) $\phi = 0.346$, (b) $\phi = 0.200$, (c) $\phi = 0.100$, where the first occluded volumes of conductor have begun to develop, and (d) $\phi = 0.030$, near the percolation threshold. The insulating spheres (white) grow out of the conducting diphasic medium (black).

areas of interfacial contacts grow, creating an ever decreasing volume of pores and throats, which contains the remaining two phase mixture (Fig. 3(c)). Finally, when the volume fraction (f) of the insulating spheres is about 0.97 (Fig. 3(d)), the throats no longer form a percolation path [11]. This would give a ϕ_c of approximately 0.03, if the material remaining in the pores and throats is the pure conducting phase. An even lower ϕ_c would be obtained if the insulating ''spheres'' stopped growing for f of about 0.97, leaving a conducting two phase composite in the just percolating pores and throats. For a medium where the radius of the insulating particles is very much larger than that of the conducting particles, the value of ϕ_c for R_I/R_C (radius insulating sphere/radius conducting sphere) was first calculated on the basis that each non-conducting grain is covered with a monolayer of conducting particles at ϕ_c. Later it was realized that the conducting particles did not have to cover the insulating particles completely, but had only to form a percolation path [12]. In this case a two dimensional percolating network is formed at a ϕ_c, which is about one-half [9] of that needed for the completely covered insulating particle model. It was also realized [12] that the conducting particles are not only on the surface of the insulating grains, but also trapped in the interstitial sites or pores, which increases the observed value of ϕ_c. Both theoretical minimum and practical minimum values of ϕ_c for each value of are given in [12]. A practical minimum for R_I/R_C is 30, which gives, after making allowance for the conducting phase trapped in the pores, a ϕ_c of about 0.03.

Still another method of achieving a very low ϕ_c is to use filler particles with an elongated geometry or high demagnetization coefficient (rods or discs) [13]. This has been done by Carmona and co-workers [14] who studied the difference in the ϕ_c obtained for a carbon powder and for randomly oriented carbon fibers, with various length-to-cross-section ratios, bonded in epoxies and silicon elastomers.

To have ϕ_c larger than 0.16 one must visualize a medium where all the grains (sites in lattice theories) do no form electrical contacts (bonds in lattice theories) with their nearest neighbors. (Recall that if all the neighboring grains, of roughly equally size, are electrically connected, ϕ_c is about 0.16.) However, if some of the nearest-neighbor conducting grains fail to make electrical contact (in practice, often due to the insulating component tending to but not completely wetting and covering the grains), the critical volume fraction would rise above 0.16. This is a site-bond percolation situation in lattice theory [4]. Note that the volume fraction for space filling and touching spheres on a regular closely packed lattice, or placed at random (Fig. 3(b) with the conducting grains black), lies between 0.52 (simple cubic) and 0.74 (face centered cubic) [9]. Therefore this range can be visualized as an upper limit for ϕ_c in a mixture, when the insulating phase does not completely wet and or cover the conducting grains.

IV. Scaling and the Percolation Equations

Good percolation systems are characterized by a smooth and rapid change of the dc electrical conductivity in a narrow range of conductor volume fractions. It has been well established, both experimentally and theoretically, that near the percolation threshold ϕ_c, the dc conductivity $\sigma(\phi, 0)$, ϕ being the volume fraction of conductor, follows the power-laws $\sigma(\phi,0)\alpha(\phi-\phi_c)^t$ as ϕ_c is approached from the conducting side $(\phi>\phi_c)$, with t as the conductivity exponent, and $\sigma(\phi,0)\alpha(\phi_c-\phi)^{-s}$, where the exponent s describes the divergent behavior of the conductivity, when ϕ_c is approached from the insulating side $(\phi<\phi_c)$. The real part of the low frequency dielectric constant $\varepsilon(\phi,\ \omega\ \approx\ 0)$ of percolation systems is also predicted to diverge as $\varepsilon(\phi)\alpha|\phi_c-\phi|^{-s'}$, where s' is the dielectric exponent, on both sides of ϕ_c [5–7]. A s and a s' are introduced in Wu and McLachlan [15,16] as they are found to be different from experiments performed on some Graphite-Boron Nitride systems. From early results for computer simulations, model experiments and some continuum systems, the critical exponents t and s were first thought to be universal, i.e., they depended only on the dimension of the percolation system (which would require $s = s'$, which is not always observed [15]) and not on the details of cluster geometry and inter granular contacts. This is now known not to be true for some continuum systems [5,6,15].

The complex ac conductivity $\sigma(\phi, \omega)$, or dielectric constant $\varepsilon(\phi, \omega)$, for percolation systems are usually arrived at using a scaling ansatz for the complex ac conductivity $\sigma_m(\phi,\omega)=\sigma_{mr}(\phi,\omega)-i\omega\varepsilon_o\varepsilon_{mr}(\phi,\omega)$ [5–7]. The same scaling ansatz gives higher order terms for the dc conductivity. The scaling equations can be written as

$$\sigma_m(\phi,\omega)\alpha\sigma_{cr}(\phi-\phi_c)^t F_+(x \text{ or } i\omega/\omega_c)$$

and

$$\sigma_{cr}(\phi_c-\phi)^t F_+(x \text{ or } i\omega/\omega_c) \tag{5}$$

where F_+ and F_- are the complex scaling functions above and below ϕ_c and σ_{cr} is the real component of the conductivity σ_c of the more conducting and very dominant component above ϕ_c. x and ω_c, the critical or scaling angular frequency, are given by

$$x=(\sigma_i/\sigma_c)|\phi-\phi_c|^{-s-t}$$

and $\quad \omega_c=(\sigma_c/(\varepsilon_o\varepsilon_t))|\phi-\phi_c|^{t+s}$

$$(\propto \sigma(\phi,0)^{(t+s)/t}) \tag{6}$$

Note ω_c is only defined for a conducting phase where $\sigma_{ci}=0$ and where $\sigma_{ii}=i\omega\varepsilon_0\varepsilon_r$ and $\sigma_{ir}=0$. Using Eqs. (5) and (6), σ_m and σ_{mr} can be written as [5–7],

$$\sigma_{mr}(\phi)=A'_+\sigma_c(\phi-\phi)^t+B'_+\sigma_{cr}(\phi-\phi_c)^{-s}$$

and

$$B'_-\sigma_{ir}(\phi_c-\phi)^{-s}+C'_-(\sigma_{ir}^2/\sigma_{cr})(\phi_c-\phi)^{-2s-ti}: \tag{7a}$$

$$\sigma_m(\phi,\omega)=A^*_+(\phi-\phi_c)^t+B^*_+\omega(\phi-\phi_c)^{-s}$$

and

$$B^*_-\omega(\phi_c-\phi)^{-s}+C^*_-\omega^2(\phi_c-\phi)^{-2s-t} \tag{7b}$$

for ϕ above and below ϕ_c respectively. (Note in the percolation equations one is using σ_c and σ_i while in the effective media equation σ_h and σ_l were used.)

The first term in Eq. (7a) is the well known equation for the dc conductivity and the $B_-\omega(\phi_c-\phi)^{-s}$ term gives $\varepsilon_{mr}\alpha(\phi_c-\phi)^{-s}$, the dielectric divergence equation. Note the imaginary parts of σ_c and ε_r of the conducting and insulating components respectively,

have been assumed to be zero in the expression for Eq. (6), therefore for the conducting component $\sigma_c = \sigma_{cr}$, and for the insulating component $\varepsilon_{ii} = 0$ and $\sigma_{ii} = -i\omega\varepsilon_o\varepsilon_{rr}$. At high frequencies for samples with ϕ close to ϕ_c and $(\omega/\omega_c) > 1$, in the RC model [5], Eq. (5) reduces to [5]–[7],

$$\sigma_{mr}(\phi, \omega) \propto (\omega/\omega_c)^u$$

and

$$\varepsilon_{mr}(\phi, \omega) \propto (\omega/\omega_c)^{-v} \tag{8}$$

$$u = t/(s+t) \text{ and } v = s/(s+t) \tag{9a}$$

u and v are two critical exponents which satisfy the following scaling relation [5–7]

$$u + v = 1 \tag{9b}$$

independent of the model used to derive u and v. The region where x or $\omega/\omega_c > 1$ and Eq. (8) is obeyed is called the crossover region. Note Eqs. (7) and (8) have arbitrary constants and only give the $|\phi - \phi_c|$ and ω dependence for x, or $\omega/\omega_c < 1$ and $x, \omega/\omega_c > 1$, which severely limits their applicability.

The following expressions can be used to obtain phenomenological analytical curves for F_+ and F_-:

$$F_+(x_+ \text{ or } \omega/\omega_{c+}) = \sigma_{GM}/\sigma_c((\phi - \phi_c)/(1 - \phi_c))^t$$

and

$$F_-(x_- \text{ or } \omega/\omega_{c-}) = \sigma_{GM}/\sigma_c((\phi_c - \phi)/\phi_c)^t \tag{10}$$

where σ_{GM} is given by [15–18],

$$(1-\phi)({\sigma_i}^{1/s} - {\sigma_{GM}}^{1/s})/({\sigma_i}^{1/s} + A{\sigma_{GM}}^{1/s}) +$$
$$\phi({\sigma_c}^{1/t} - {\sigma_{GM}}^{1/t})/({\sigma_c}^{1/t} + A{\sigma_{GM}}^{1/t}) = 0 \tag{11}$$

and $A = (1 - \phi_c)/\phi_c$. σ_i, σ_c and σ_m can, and hence F_+ and F_- as well as x_+, x_-, ω_{c+} and ω_{c-}, be real or complex. The normalizations in $(\phi - \phi_c)/(1 - \phi_c)$ and $(\phi_c - \phi)/\phi_c$, differ from those in Eq. 5, but enable curves for F_+ and F_- that are independent of ϕ_c to be obtained. If $i\omega\varepsilon_0\varepsilon_r$ is substituted for σ_i in $x_+ = (\sigma_i/\sigma_c)((\phi - \phi_c)/(1 - \phi_c))^{s+t} = \omega/\omega_{c+}$ and $x_- = (\sigma_i/\sigma_c)((\phi_c - \phi)/\phi_c)^{s+t} = \omega/\omega_{c-}$, this gives

$$\omega/\omega_{c+} = (\omega\varepsilon_0\varepsilon_r/\sigma_c)((1 - \phi_c)/(\phi - \phi_c))^{t+s}$$

and

$$\omega/\omega_{c-} = (\omega\varepsilon_0\varepsilon_r/\sigma_c)(\phi_c/(\phi_c - \phi)),^{t+s} \tag{12}$$

which define ω_{c+} and ω_{c-} for an ideal conductor and an ideal insulator or loss free dielectric. It can be shown [17,18] that the limiting values of the first order terms of F_+ and F_- against x_+, x_-, ω/ω_{c+} and ω/ω_{c-} are,

$$F_+(x_+)(\text{and } F_+(-i\omega/\omega_{c+})) = 1$$
$$(\text{for } x_+ \text{ or } \omega/\omega_+ < 1) \tag{13a}$$

$$F_-(x_-)(\text{and } F_-(-i\omega/\omega_c)) = x_-(\omega/\omega_{c-})$$
$$(\text{for } x_- \text{ or } \omega/\omega_c < 1) \tag{13b}$$

$$F_+(x_+)(\text{and } F_+(-i\omega/\omega_{c+})) \propto {x_+}^{t/(s+t)}$$
$$((\omega/\omega_{c+})^{t/(s+t)}) \quad (\text{for } x_+ \text{ or } \omega/\omega_{c+} > 1) \tag{13c}$$

$$F_-(x_-)(\text{and } F_-(-i\omega/\omega_c)) \propto {x_-}^{t/(s+t)}$$
$$((\omega/\omega_{c-})^{t/(s+t)} \quad (\text{for } x_- \text{ or } \omega/\omega_{c-} > 1) \tag{13d}$$

All the first order terms of the above limiting expressions, derived analytically [17] and shown numerically [16–18], are the same as for the scaling functions defined [5–7]. For $x_+(\omega/\omega_+) > 1$ and $x_-(\omega/\omega_-) > 1$ there is agreement between Eqs. (13c) and (13d) and the equations given [5–7] for the second order terms. The second order terms of the function F_+ and F_- [or $\sigma_{mi}(\phi > \phi_c)$ and $\sigma_{mr}(\phi < \phi_c)$] differ from those in Eqs. (7a) and (7b) when $x_+(\omega/\omega_{c+}) < 1$ and $x_-(\omega/\omega_{c-}) < 1$. These differences are shown analytically in McLachlan et al. [17], where measurements of $\sigma_{mr}(\phi < \phi_c)$, which strongly favor Eqs. (10) and (11) are also reported.

In order for experimental results, measured as a function of two independent variables (e.g., $\phi - \phi_c$ and ω), to scale, a function of the two variables must exist such that the experimental dispersion results for a series of samples (e.g., different ϕ values) superimpose, when plotted in terms of this scaling function. In the specific case considered here, if measurements of $\sigma_m(\phi, \omega)$ are made and at every measured point plotted as F_+ or F_-, there are an infinite number of other $\sigma_m(\phi', \omega')$ points which give the same value of F_+ or F_-, provided they have a combination of ω' and ϕ' which give the same value of x_+, x_-, ω/ω_{c+} or ω/ω_{c-}.

Unfortunately exact solutions to the complex equations for $F_+(x_+)$ and $F_-(x_-)$ are not available for arbitrary s and t. However, with the values of $s = 1$ and $t = 2$, $F_+(x_+)$ and $F_-(x_-)$ can be calculated from

a complex cubic equation [17]. Any *t/s* value equal to an integer gives a polynomial equation, which can then be solved analytically [17]. This is done to provide a qualitative comparison with some of the data. Note that Eq. (9) can be solved as an implicit equation for arbitrary s and t if σ_c and σ_i are real [18]. Reference [18] also shows how the dc conductivity results, shown in Fig. 5, can be scaled into theoretical scaling curves derived using Eqs. (10) and (11).

The exponents s and t were first thought to be universal [5–7] and to depend only on the dimension (1d, 2d, 3d) of the system, with 3d values of $s = 0.87–0.89$ and $t = 2.0$. (Although in some work values in the range 1.7 to 2.0 are considered to be universal.) This is now known not to be the case. For instance in systems where various conducting powders were distributed on large insulating grains, a microstructure described earlier, values of s in the range 0.35–1.3 and t in the range 1.7–5.8 were observed [19]. The current theories for non universal exponents are all based on there being a large range or anomalous distributions of the conductances between the particles and clusters. There are analytic models for some specific structures and one based on intergranular (cluster) tunneling. There is also evidence that extreme shapes, such as rods, of the conducting grains can give high t values [14]. For further details on non-universality the reader is referred to the discussions and references in Bergman and Stroud [5] and Nan [6].

V. Experimental Results and Simulations: General

If it is at all possible the starting point for an experimental analysis of an electroceramic system should be a measurement of the dc σ_m (σ_{mr}) as a function of ϕ, on both sides of ϕ_c. After an examination of these results, and a comparison with a figure similar to Fig. 2, it should be possible to decide if the system has a continuous or grain coating matrix (BA curves b and d or MW-HS curves a and e) or is a percolation system displaying a curve such as c in Fig. 2. Continuous matrix systems can, in principle, be fitted using the BA, MS-HS equations or the interpolations and Bricklayer (BL) model as described in McLachlan et al. [20]. Percolation results should be analyzed using the two exponent GEM equation for σ_{GM} or the first order percolation equations for σ_m, on both sides of ϕ_c and with a common ϕ_c, to obtain ϕ_c, s and t. Examples of such fits are given in Fig.4 $(\sigma_c/\sigma_i \ggg 1)$ [15] and Fig. 5 $(\sigma_c/\sigma_I > 1)$ [21]. (Note that a fit of results on the

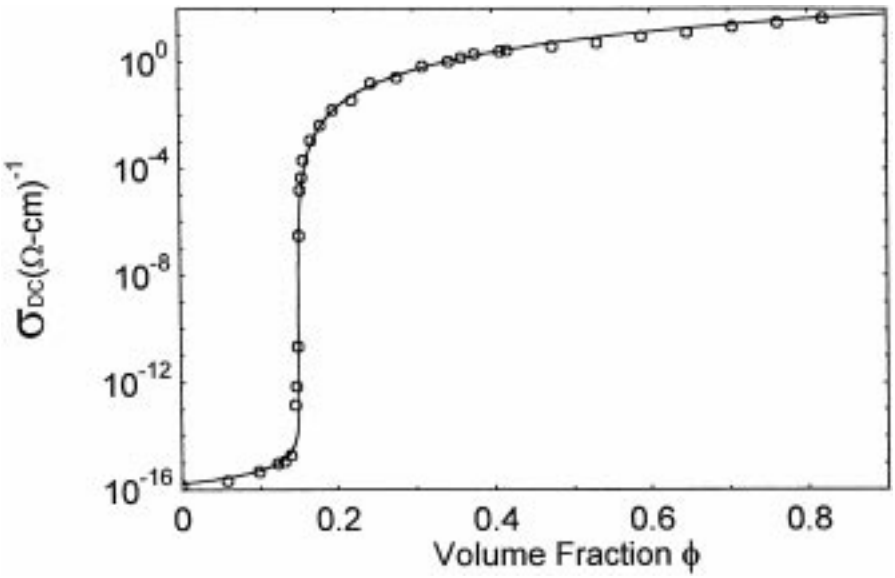

Fig. 4. This figure shows a plot of the experimental resistivity results for Graphite–BN composites as a function of the volume fraction. The theoretical fit is obtained using the GEM equation (Eq. (11)) with the following parameters: $\phi_c = 0.150$, $\rho_i = 7.24 \times 10^{15}$ Ω cm, $\rho_c = 0.13$ Ω cm, $s = 1.05$ and $t = 3.03$.

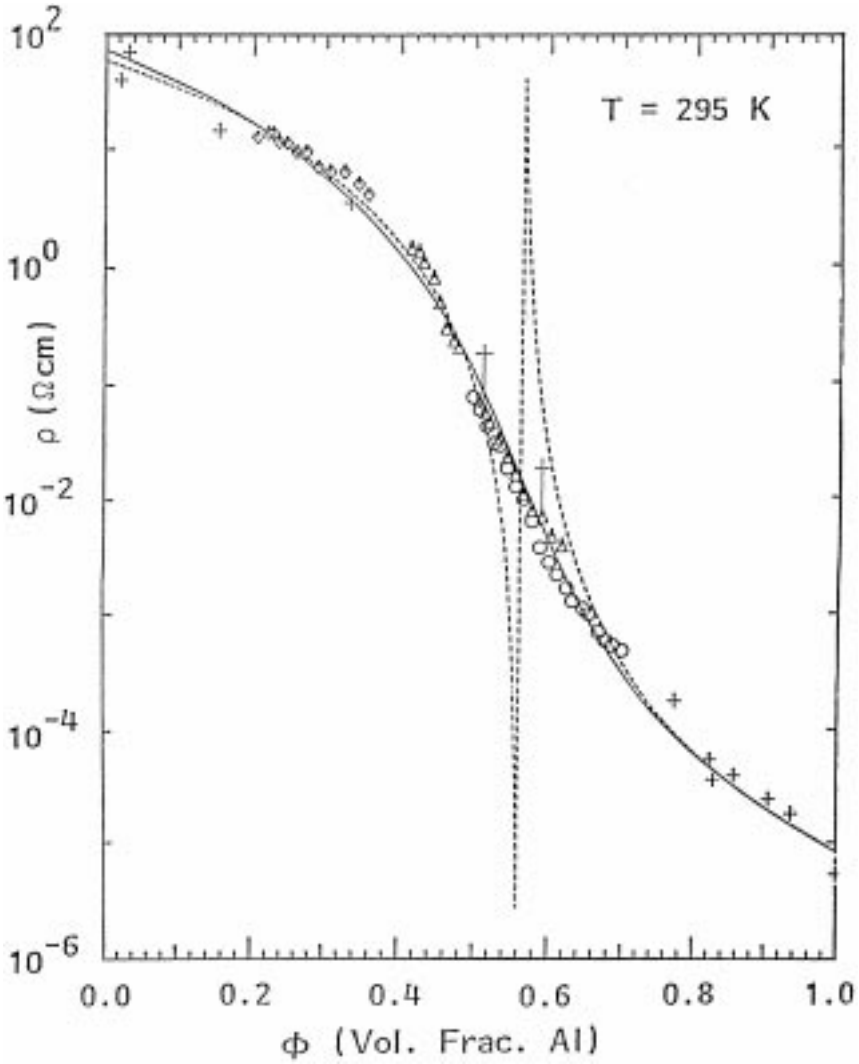

Fig. 5. A plot of experimental and theoretical resistivities versus Aℓ volume fraction ϕ at 295 K. The full curve is a plot of the GEM equation (Eq. 11) and the broken curves are plots of the percolation equations given in Eq. (7a). The parameters used in these plots GEM: $\phi_c = 0.56$, $s = 2.9$ and $t = 3.35$ and perc. Eqs.: $\phi_c = 0.56$, $s = 3.46$ $t = 3.46$. The daggers indicate the range of experimental points closest to ϕ_c not incorporated in the percolation equation fit as they are in the crossover region.

conducting side only often gives a number of nearly equally good $\phi_c - t$ combinations.)

If the high conductivity component goes superconducting, ϕ_c may, in principle, be determined very accurately from measurements below T_c. However, due to electron tunneling the results are not as straightforward as it might appear. For further information and results regarding such superconducting measurements the reader is referred to McLachlan et al. [21], Eytan et al. [22] and Shoskany et al. [23].

In ac measurements, such as impedence spectroscopy (IS), it is often not the magnitude of σ_{mr} and σ_{mi} (or ε_{mr} and ε_{mi}) that provides a clue to the microstructure but the dispersion shown by both $\sigma_{mr}(\omega)$ and $\sigma_{mi}(\omega)$. The dispersion arises from the properties of the components and/or the microstructure. The dispersion that occurs in the BA, MW-HS & BL systems for continuous grain coated matrix, takes place only at and between the angular frequencies, $(\sigma_{hr}/(2\pi\varepsilon_{hr}\varepsilon_0)$ and $\sigma_{\ell lr}/(2\pi\varepsilon_{\ell lr}\varepsilon_0)$ characterizing the components, with their relative amplitudes being

determined by the volume fractions. This places restrictions on the components upon which and the temperatures at which such measurements can be made. As, in practice, the frequencies available in dielectric spectrometers goes from 10^{-3} Hz to 10^{9} Hz and, taking a typical $\varepsilon_r = 6$, which gives $\varepsilon_r\varepsilon_0 = 5.31 \times 10^{-11}$, this requires the range of resistivities to lie between $3 \times 10^{10}\,\Omega\,\text{cm}$ and $3 \times 10^{-2}\,\Omega\,\text{cm}$. Therefore measurements are often made at high temperatures in order to decrease the resistivity of one or both of the components. The lower resistivity limit means that complete IS measurements cannot be made satisfactorily, even with conductors such as carbon and Graphite. Impedance Spectroscopy is discussed in the next section.

On the other hand percolation systems show different dispersion relationships for $\sigma_{mr}(\omega)$ and $\sigma_{mi}(\omega)$ above and below ϕ_c (with $x_+, \omega_+, x_-, \omega_- < 1$) and in the crossover region $(x_+, \omega_+, x_-, \omega_- > 1)$ which can, in principle, be used to determine the percolation parameters of a system, possibly even for a single sample. As experimenters have, in the past, been mainly concerned with proving certain aspects of percolation theory, they have usually used components with characteristic frequencies outside of the range given in the last paragraph and certainly well outside the frequency range of their instrument(s). Recall that Eqs. (6) and (12) for ω_c, ω_{c+} and ω_{c-} are for ideal insulators and conductors and the components used to test these equations should have $\sigma_{cr} \ggg \sigma_{ci}$ (or $\omega\varepsilon_0\varepsilon_{cr}$) and $\sigma_{ii}(\omega\varepsilon_0\varepsilon_{ir}) \ggg \sigma_{ir}$. Dispersion relations for percolation systems are usually presented as plots of σ_{mr} and ε_{mr} versus the log of ω or the frequency.

VI. Experimental Results and Simulations: Effective Media Systems

As this subject was covered in detail in a recent publication [20], only a few illustrative figures and salient points will be given in this section, which is primarily concerned with impedance spectra, which are routinely used to characterize the inhomogeneous microstructure from the electrical transport properties of ''composite'' electroceramics. The simplest spectra to understand are for two component or phase systems where the one component coats the other. The one component should have a significantly lower or higher conductivity than the other. The coating component could be grain boundaries, with a very small volume fraction, or a true second phase distributed uniformly, at the interfaces of the granular component, with a continuous 3D connectivity and a volume fraction that can range from very small to nearly one. The MW-HS, BA and other [20] equations should be able to be used to model and perhaps even fit results in both these cases.

In order to demonstrate that the above equations do produce the type of impedance spectra that are observed in practice, a few computer simulations are given here and more in McLachlan et al. [20]. Impedance spectra are usually plotted giving the imaginary component as a function of the real component of the impedance and sometimes the modulus, but very rarely as the admittance or capacitance. Therefore, in this paper the complex conductivity σ_m^*, as obtained from the above equations as a function of ω for fixed ϕ, was converted to the impedance (Z) or modulus (M) using the following equations,

$$\begin{aligned} Z_{mr} &= GF(\sigma_{mr}/(\sigma_{mr}{}^2 + \sigma_{mi}{}^2)) \\ \text{and} \quad M_{mr} &= \omega Z_{mr} \\ Z_{mi} &= GF(\sigma_{mi}/(\sigma_{mr}{}^2 + \sigma_{mi}{}^2)) \\ \text{and} \quad M_{mi} &= \omega Z_{mi}. \end{aligned} \tag{14}$$

GF is a geometric factor used to convert from conductivity to conductance etc. In this paper GF is chosen so that the impedance or modulus given are for a one centimeter cube of material.

The simulations plotted in the figures are for a two component system, where the more conducting component has $\sigma_{cr} = 3 \times 10^{-5}(\Omega - m)^{-1}$, $\varepsilon_0\varepsilon_{cr} = 3 \times 10^{-11}$ (Farad/m) or $\sigma_{ci} = 3 \times 10^{-11}\omega$ and a characteristic ω_c of 1×10^6 and the more insulating one has $\sigma_{ir} = 3 \times 10^{-8}(\Omega - m)^{-1}$ and $\varepsilon_0\varepsilon_r = 3 \times 10^{-11}$ (Farad/m) or $\sigma_{ii} = 3 \times 10^{-11}\omega$ and a characteristic ω_i of 1×10^3. In order to generate these plots ω was allowed to vary between 1 and 10^9. These conductivity parameters, with a single relaxation time, lead to semi-circular arcs. If the conductivity equations [24,25] that give depressed arcs had been used for the two components, then depressed arcs would be observed in all the simulations given below. Single relaxation time components are used here and in McLachlan et al. [20] in order to see if any arc

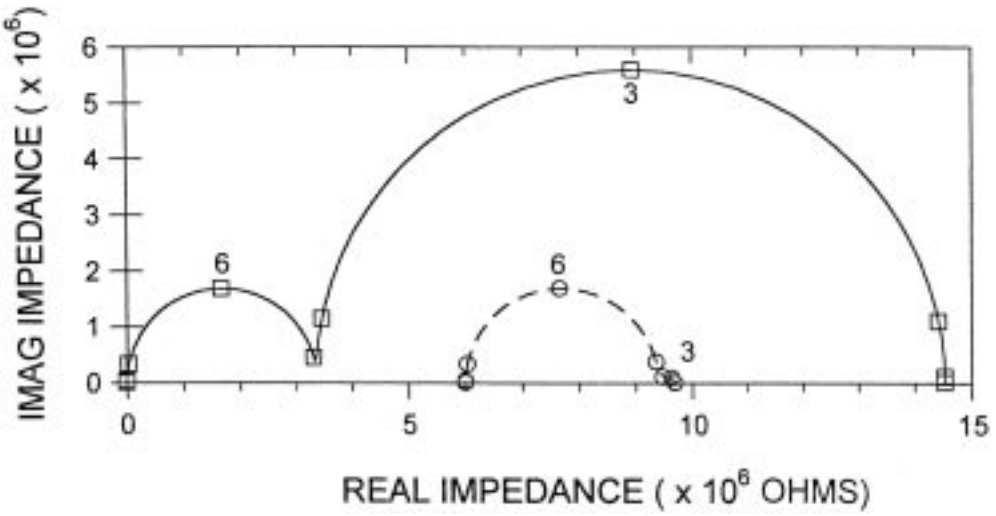

Fig. 6. The imaginary impedance (Z_{mi}) plotted against the real impedance (Z_{mr}) using the MW (—), and BA (- - - -) equations, with $\phi = 0.99$. The conducting component has $\sigma = 3 \times 10^{-5}\ (\Omega - \mathrm{m})^{-1}$ and $\varepsilon_o \varepsilon_r = 3 \times 10^{-11}$ (Farad/m) and the insulating component $\sigma = 3 \times 10^{-8}\ (\Omega - \mathrm{m})^{-1}$ and $\varepsilon_o \varepsilon_r = 3 \times 10^{-11}$ (Farad/m). The exponent of ω is given at certain key points on the plots.

distortions arise, due to the microstructures that form the basis of the above equations.

Systems in which the matrix or coating phase is insulating often give double arcs, one for each component. Figure 6 shows impedance plots for a conducting grain volume fraction of 0.99, which clearly illustrates the double arcs obtained from the MS-HS and BA equations (Eqs. (2) and (3)), with the exponent of certain ω values indicated. The width of the low frequency arc indicates the impedance due to the insulating phase and the high frequency arc the conducting phase. Naturally as ϕ decreases the width of the low frequency arc increases until the high frequency arc becomes unobservable. For comparison

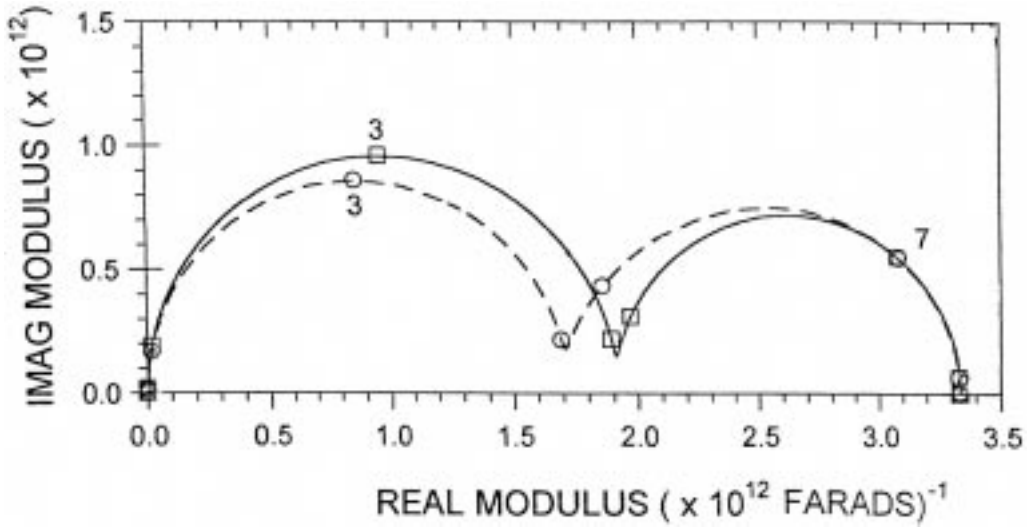

Fig. 7. The imaginary modulus (M_{mi}) plotted against the real modulus (M_{mr}) using the MW (—), and BA (- - - -) equations, with $\phi = 0.20$. The conducting component has $\sigma = 3 \times\ 10^{-5}\ (\Omega - \mathrm{m})^{-1}$ and $\varepsilon_o \varepsilon_r = 3 \times 10^{-11}$ (Farad/m) and the insulating component $\sigma = 3 \times 10^{-8}\ (\Omega - \mathrm{m})^{-1}$ and $\varepsilon_o \varepsilon_r = 3 \times 10^{-11}$ (Farad/m). The exponent of ω is given at certain key points on the plots.

purposes, the Bruggeman Asymmetric model has been shifted away from the origin in Fig. 6. The shifted BA arc has a very similar high conductivity arc and a very small low conductivity arc. This suggests that in this BA microstructure the infinite size range of conducting spheres must lie much closer to each other than in the MW microstructure and that they effectively short-out the insulating medium. This would appear to be consistent with the microstructures shown in Fig. 1.

The high conductivity arcs for the MW and BA media are similar. This is because the current maximizes its path in this component so as to obtain the required minimum resistance for or power dissipation in the two phase composite. The very different arcs characterizing the low conductivity component in the MW and BA media show that the size of the low conductivity component arc depends critically on microstructure, even in media where the low conductivity component obviously coats the high conductivity component and forms a continuous matrix component.

Fig. 7 shows plots of real modulus (M_{mr}) against imaginary modulus (M_{mi}) (Eq. (14)), for a conducting volume fraction of 0.2. Note that for this value of ϕ, an impedance plot (Z_{mi} vs. Z_{mr}) does not give separated arcs and that it is important to examine both impedance and modulus plots.

In the case where conductor coats the more insulating spheres (i.e., a conductor matrix system) only single arcs are observed for all ϕ values. It is observed [20] that the peak ω of the semi-circular arcs characterizing these conductor matrix media moves from 10^3 to 10^6 as ϕ goes from nearly zero to one. The single arc means that the separate contributions of the two components to the impedance or modulus cannot differentiated by means of IS plots.

VII. Experimental and Simulations: Percolation Systems

The system chosen to illustrate dispersion in percolation systems is a lightly poured powder consisting of 55% Graphite: 45% Boron Nitride and air under going a stepped compression [16]. Examples of other systems which display similar behavior are given in Wu and McLachlan [16] and Chiteme and McLachlan [19] and the references in Wu and McLachlan [16].

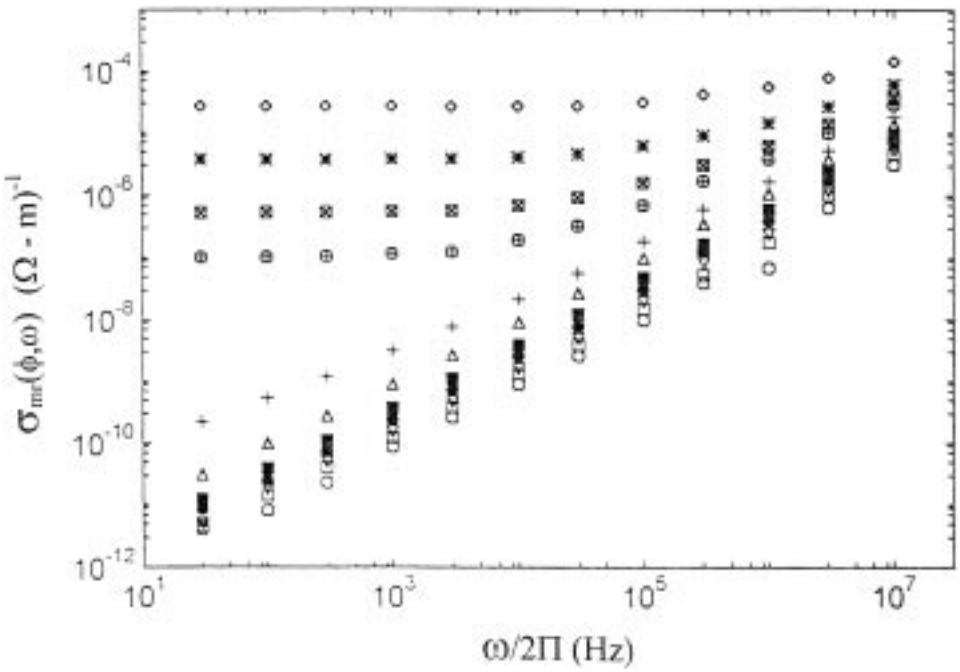

Fig. 8. A plot of the conductivity $\sigma_{mr}(\phi,\omega)$ against frequency for a 55% G:45% BN powder in air, on a log:–log scale, for various of ϕ. $\phi = 0.133$ (diamond), 0.129 (star), 0.127 ($\times$ in box), 0.125 (plus in box), 0.123 (plus), 0.121 (triangle), 0.120 (dark square), 0.118 (dark circle), 0.116 (inverted triangle), 0.115 (open square), 0.112 (open circle). Note that $\phi_c = 0.124$.

The results from the dc conductivity and low frequency ac dielectric measurements as a function of ϕ experiments, on both sides of ϕ_c, have been given in Fig. 4 and Wu and McLachlan [15]. The values of s, t and ϕ_c obtained from these measurements were used to calculate the F_+ and F_- plots given below, which are therefore independent of the dispersion measurements reported in this paper.

Figure 8 shows the ac conductivities $(\sigma_{mr}(\phi,\omega))$ versus the frequency on a log–log scale, for a 55% G : 45% BN powder in air system. For $\phi \leq \phi_c$, the conductivities increase approximately linearly over the entire frequency range. Well above ϕ_c, the conductivity shows no dispersion in the low frequency range. A ''dc–ac'' crossover or critical frequency ω_{c+} exists, beyond which the conductivity starts to increase with frequency and eventually, in some cases for ϕ very close to ϕ_c, shows a linear region on a log–log plot, at higher frequencies. The crossover frequency ω_{c+} increases continuously as $(\phi - \phi_c)$ or σ_c increases (Eqs. (6) and (12)). It should be noted that, at high frequencies, there is very little difference in the exponent for the power law describing the dispersion of the insulating and conducting samples close to the critical volume fraction, as required by Eqs. (13c) and (13d). The lack of dispersion in the

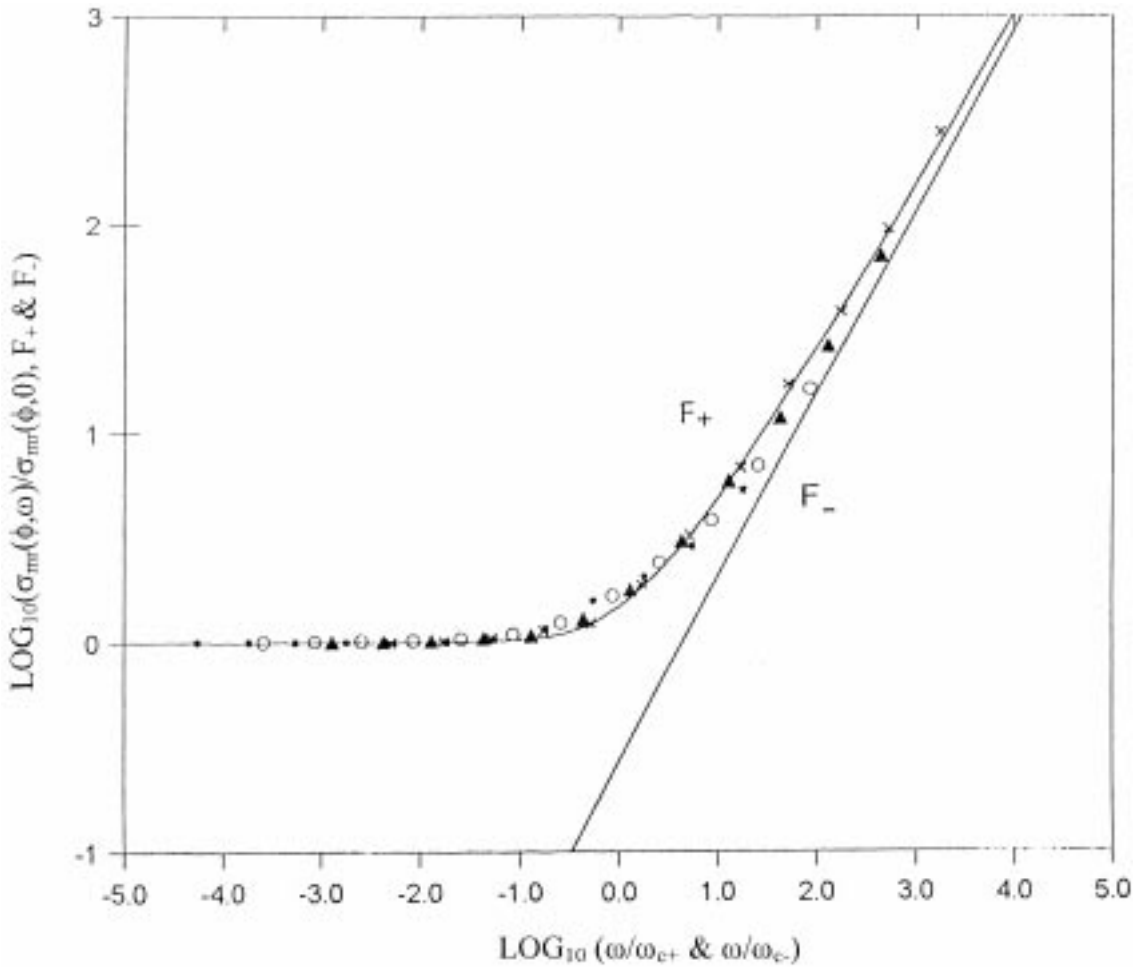

Fig. 9. A plot of the log of the scaled conductivities $\sigma_{mr}(\phi,\omega)/\sigma_m(\phi,0)$ against the log of the scaled frequency (ω/ω_{c+}) or (ω/ω_{c-}) for a 55% G : 45% BN powder. The origin of the F_+ and F_- plots, onto which the experimental curves are scaled along the (ω/ω_{c+}) or (ω/ω_{c-}) axis, are discussed in the text. The parameters used are $\sigma_c = 3116\ (\Omega\ \mathrm{m})^{-1}$, $\sigma_i = 2.92 \times 10^{11}\omega\ (\Omega - \mathrm{m})^{-1}$, $s = 0.72$, $t = 4.8$ and $\phi_c = 0.124$.

low-frequency range distinguishes a conducting sample ($x_+ < 1$) from an insulating one ($x_- < 1$) or one in the cross over region ($x_+, x_- > 1$).

According to the scaling laws, the scaled experimental results on the conducting side of percolation ($\phi > \phi_c$) depend only on ω/ω_{c+}. Figure 9 shows the reduced ac conductivity $\sigma(\phi,\omega)/\sigma(\phi,0)$ for $\phi > \phi_c$ versus the reduced frequency ω/ω_{c+}. Here the $\sigma(\phi,\omega)$ [16] and $\sigma(\phi,0)$ [15] values used are both the measured values, but $\sigma(\phi,0)$ could have been calculated from the expression linking F_+ and σ_{GM} in Eq. (10). To obtain this scaling plot, $1/\omega_{c+}$ had to be treated as a fitting parameter for each sample and empirically selected so as to make (by ''sliding'' the normalized results along the $\log \sigma(\phi,\omega)/\sigma(\phi,0) = 0$ axis) all the experimental curves lie on the analytic scaling F_+ curve, obtained using Eqs. (10)–(12). In the region $\omega/\omega_{c+} > 1$, all results obey the power-law $\sigma(\phi,\omega)/\sigma(\phi,0) \propto (\omega/\omega_c)^u$, with $u = 0.82 \pm 0.02$. The line through the data is a line obtained using the dc scaling expression (real) for $F_+(\omega/\omega_{c+} \equiv x_+)$ from Eqs. (10)–(12) with σ_c (conductor) $= 3126\,(\Omega - m)^{-1}$, σ_i (insulator) $\equiv \omega \times 3.3 \times \varepsilon_0 = \omega 2.92 \times 10^{-11}(\Omega - m),^{-1}$ $t = 4.8$, $s = 0.72$ and $\phi_c = 0.124$, all these values being obtained from Wu and McLachlan [15]. The dc scaling expression is identical to the first order term for a complex F_+, where F_+ can be evaluated for arbitrary s and t.

The variations of the ac axial dielectric constant as a function of frequency for the samples on insulating side of ϕ_c are shown in Fig. 10. As expected the dielectric constant increases with decreasing $(\phi_c - \phi)$ for all frequencies and the dielectric constant of samples with ϕ somewhat below the critical volume fraction remains constant in this frequency range. Recent experimental measurements [19] show that the exponent s, when obtained from low frequency ac susceptibility as a function of ϕ measurements, is a function of frequency. For fixed ϕ, the samples closer to ϕ_c show a small negative slope $(-v)$ as expected from Eq. (8). Figure 11 shows the scaled imaginary complex ac conductivity results, plotted against ω/ω_{c-} on a log–log scale. The experimental points were obtained by first dividing the experimental $\sigma_{mi}(\phi,\omega)$ values by the *calculated* dc conductivity $\sigma_{mr}(\phi,0) = \sigma_{cr}((\phi_c - \phi_c)/\phi_c)^t$, which links σ_{GM} and F_- in Eq. 10, using the σ_c, ϕ_c and t values obtained

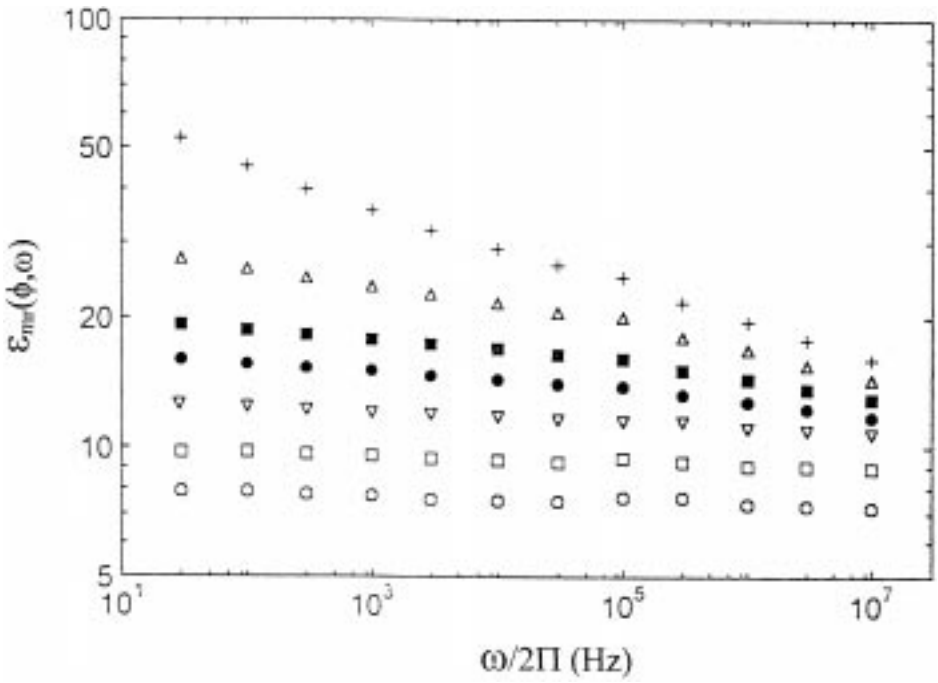

Fig. 10. A plot of the real part of the dielectric constant $\varepsilon_{mr}(\phi,\omega)$ against frequency for a 55% G : 45% BN powder in air, on a log–log scale for various values of ϕ. $\phi = 0.123$ (plus), 0.121 (open triangle), 0.120 (dark square), 0.118 (open circle), 0.116 (inverted triangle), 0.115 (open square), 0.112 (open circle). Note that $\phi_c = 0.124$.

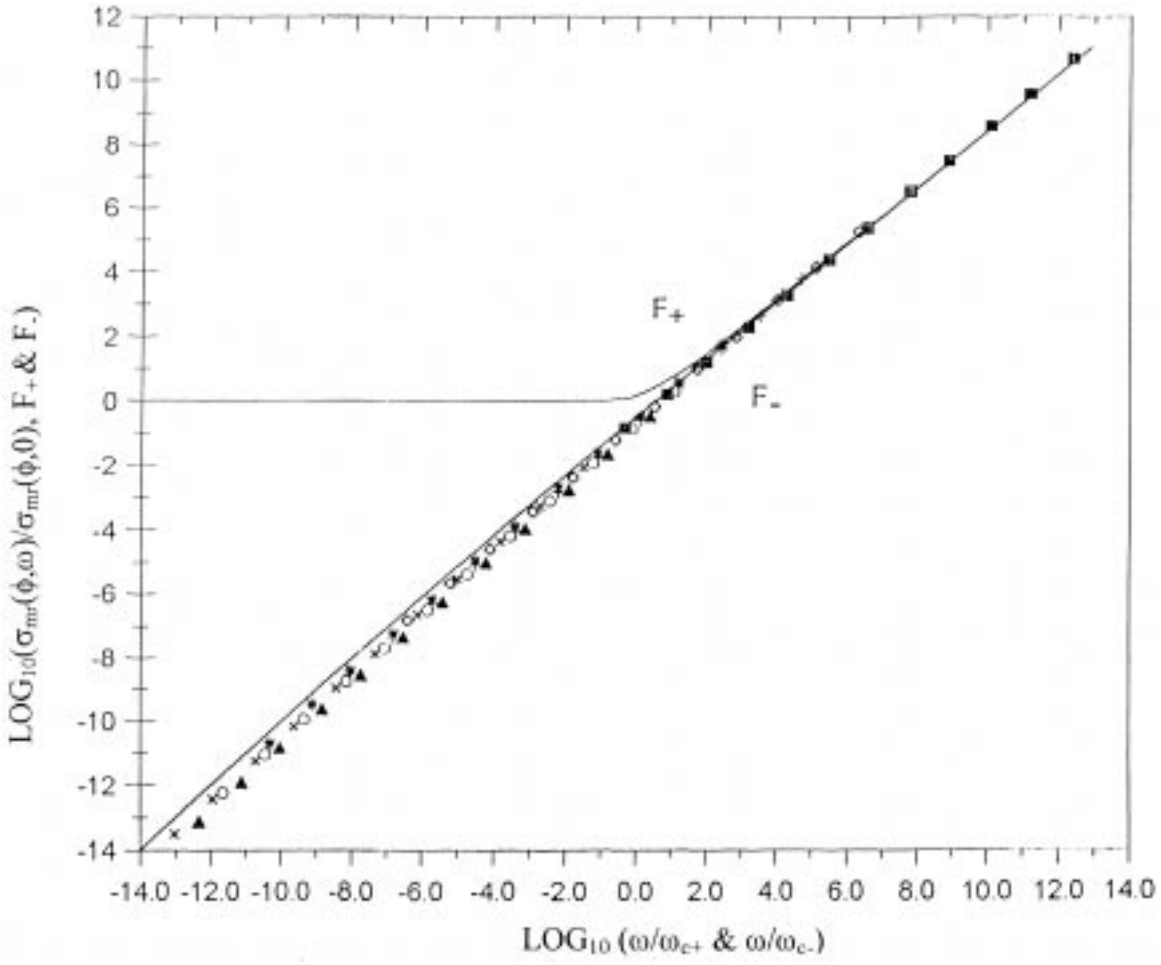

Fig. 11. A plot of the log of the scaled conductivities $\sigma_{mr}(\phi,\omega)/\sigma_m(\phi,0)$ against the log of the scaled frequency (ω/ω_{c+}) or (ω/ω_{c-}) for a 55% G : 45% BN powder. The origin of the F_+ and F_- plots onto which the experimental curves are scaled along the (ω/ω_{c+}) or (ω/ω_{c-}) axis are discussed in the text. The parameter used are $\sigma_c = 3116\,(\Omega\mathrm{m})^{-1}$, $\sigma_i = 2.92\times10^{11}\omega\,(\Omega-\mathrm{m})^{-1}$, $s = 0.60$, $t = 4.8$ and $\phi_c = 0.124$.

from the dc measurements. The dc F_- (real) curves used here and the first order (imaginary) term of a complex F_- are found to be identical, where a complex F_- can be evaluated. Note that this $\sigma_{mr}(\phi,0)$ is not a measured or measurable quantity. These normalized experimental results were then scaled by an empirical $1/\omega_{c-}$ so as to all lie on the $F_-(\omega/\omega_{c-} \equiv x_-)$ curve obtained from Eqs. (10)–(12). Note that, as required by Eqs. (13b) and (13d) and [5–7], the slope of the first order term of F_- is one for ω/ω_{c-} or $x_- < 1$ and $t/(s+t)$ for ω/ω_{c-} or $x_- > 1$. Here the parameters used are those given for the F_+ curve but with $s = 0.60$ to get a better agreement with the slope $(t/(s+t))$ of the data for $\omega/\omega_c > 1$. Note that 0.60 is the mean of the dielectric $s = 0.72$ and the dc conductivity $s = 0.47$ [15].

Although these results look very good there are serious problems. The slopes of the experimentally determined ω_{c+} plotted against the measured and calculated $\sigma_m(\phi,0)$ and ω_{c-} plotted against the calculated $\sigma_m(\phi,0)$, which should give a slope of $(t+s)/t$, are all lower than expected and the actual values of ω_{c+} and ω_{c-} are often orders different from the calculated ones [16].

The loss, or σ_{mr} below ϕ_c, term is further investigated in McLachlan et al. [17] using a better dielectric spectrometer than was available for the measurements reported in Wu and McLachlan [16].

The plotted results looked very similar to those shown in Fig. 8. These results where examined using the two dielectric loss terms, for $\phi < \phi_c$, derived in McLachlan et al. [17] from Eq. (11), which are the loss in the dielectric component and the ''percolation'' loss in the graphite clusters. The results at higher frequencies, after the elimination of the dielectric (BN) loss, give slopes of 1.05–1.09, which is somewhat lower than the $(1+t)/t((1+4.8)/4.8)$ value of 1.21 expected from the theory using the measured t value of 4.8 [15] and very different from the exponent given in Eq. (7b).

Dispersion results in systems with a percolative microstructure, but done over a frequency range which includes the characteristic frequency of one or both of the components, will obviously be very different from any that have yet appeared or been understood in the literature. In order to predict or analyze the results from such a system one needs an analytic expression such as the GEM or BS equations. Once one includes the two exponents and an arbitrary ϕ_c in the GEM equation, there are far too many possibilities to discuss in this paper. Therefore, the BS equation will be used, with $A = 2$ (spherical grains) to obtain an idea of what may be observed in percolation systems. Added advantage is that the microstructure is

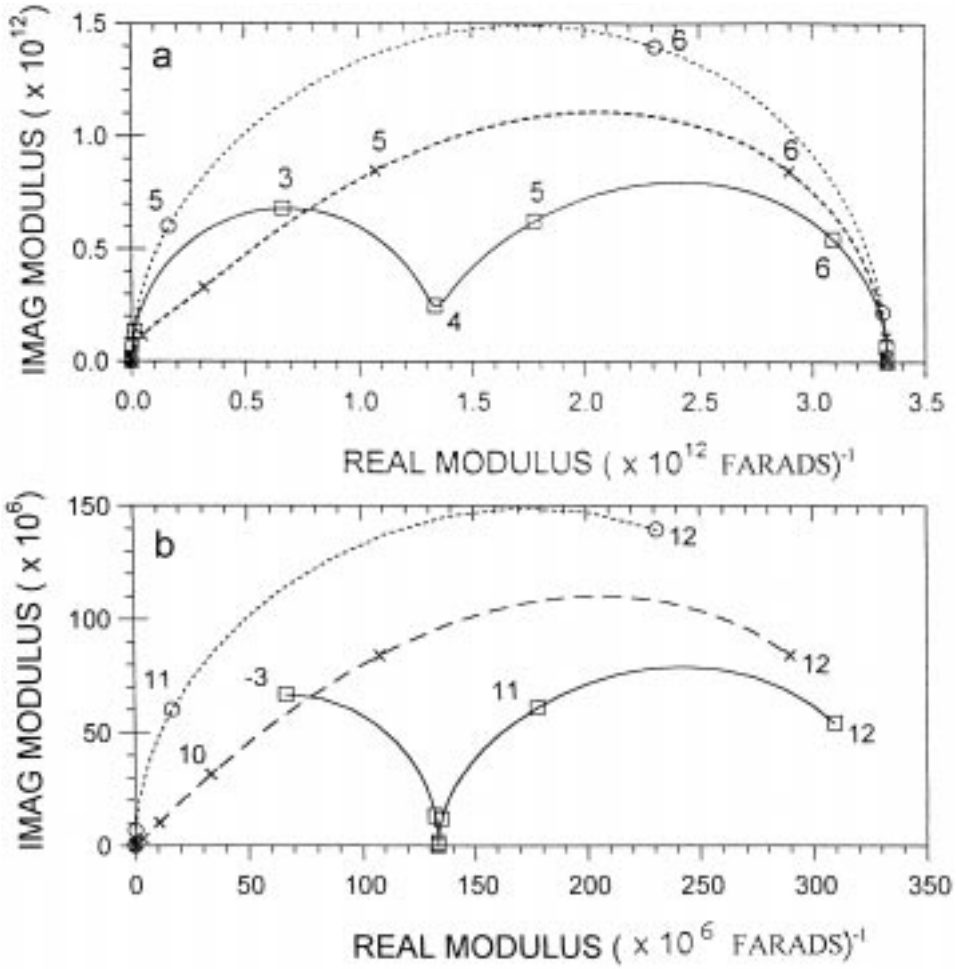

Fig. 12a and b. The imaginary modulus (M_{mi}) plotted against the real modulus (M_{mr}) using the BS equation, with $\phi = 0.20$ (—), 1/3 (– – ––) and 2/3 (· · · · · · · · ·). In Fig. 12a the conducting component has $\sigma = 3 \times 10^{-5}$ $(\Omega - \mathrm{m})^{-1}$ and $\varepsilon_o \varepsilon_r = 3 \times 10^{-11}$ (Farad/m) and the insulating component $\sigma = 3 \times 10^{-8}$ $(\Omega - \mathrm{m})^{-1}$ and $\varepsilon_o \varepsilon_r = 3 \times 10^{-11}$ (Farad/m). In Fig. 12b the conducting component has $\sigma = 30$ $(\Omega - \mathrm{m})^{-1}$ and the insulating component $\sigma = 3 \times 10^{-14}$ $(\Omega - \mathrm{m})$. $\varepsilon_o \varepsilon_r = 3 \times 10^{-11}$ (Farad/m) for all components. The exponent of ω is given at certain key points on the plots.

well defined (see Fig. 1), the BS equation is a special case of the GEM equation ($s = t = 1$ and $\phi = 1/3$) and that this will complete the discussion on the effective media theories.

Figure 12(a) shows plots of the imaginary versus real modulus for the same two components as used in Figs. 6 and 7. For $\varphi = 0.2$ the insulating component is continuous and the conducting component consists of isolated clusters. This again shows that dual arc spectra characterize media where the conducting component is completely surrounded or coated by the insulating one. For $\phi = 1/3$, where the conducting component first forms a continuous network or infinite cluster, a distorted arc, due only to the microstructure, is observed. For $\phi = 2/3$, where the insulating component becomes discontinuous, the single semicircular arcs, which characterize continuous conducting matrices in MW-HS and BA systems are observed. In the modulus plots in Fig. 12(b), the conductivity of the conducting component has been increased by 10^6 (new characteristic $\omega = 10^{12}$) and the conductivity of the insulating component has been decreased by 10^6 (new characteristic $\omega = 10^{-3}$), which should give rise to percolative dispersion in the range $1 < \omega < 10^9$. (To obtain these plots ω is varied from 10^{-3} to 10^{12}). The surprising feature, seen in Figs. 12(a) and 12(b) is that the modulus arcs are both virtually identical in shape, but with different scales, and that the ω markers have moved. Note that the characteristic ω markers of the very different high and low conductivity components coincide. Lastly, Fig. 13 shows the dispersion displayed by the conductivity in the two cases. In the first case (dashed line and $\sigma = 3 \times 10^{-5}$ and $3 \times 10^{-8} (\Omega - m)^{-1}$), dispersion only occurs between the characteristic ω's of the components, for all ϕ values. In the second case (solid line and $\sigma = 3 \times 10^{-14}$ and $30 (\Omega - m)^{-1}$) at $\phi = 1/3$, the

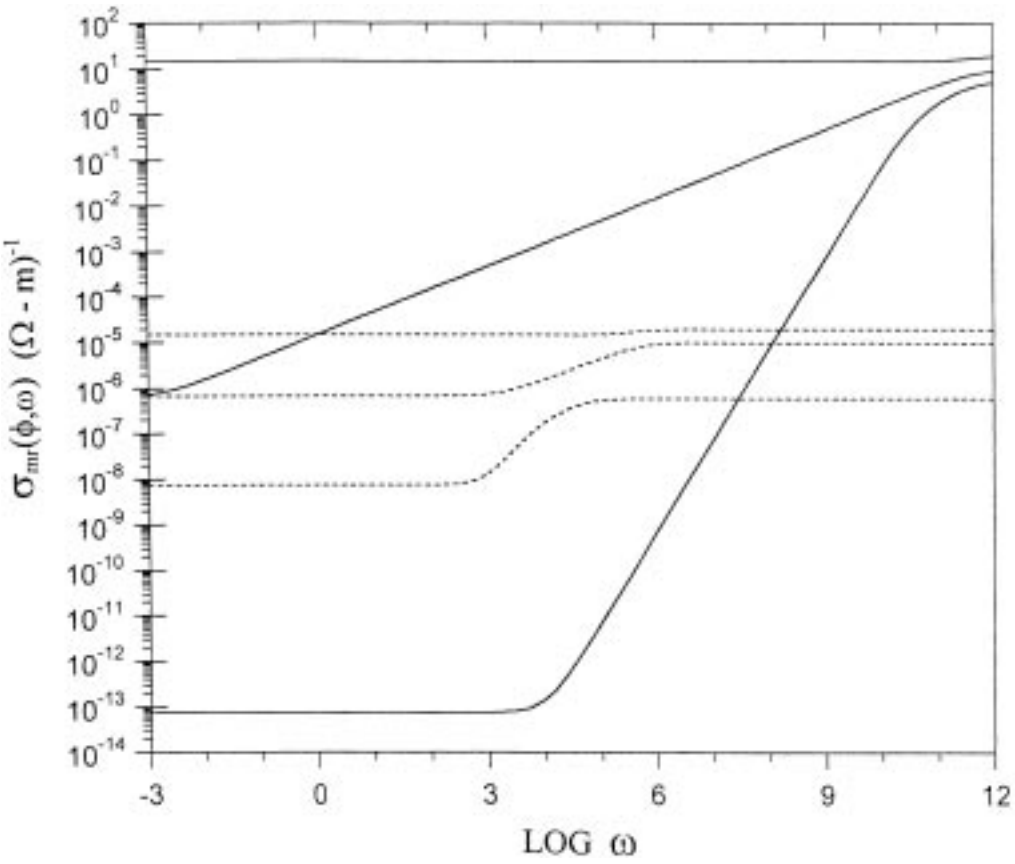

Fig. 13. This figure shows plots of the conductivity against $\log_{10}$ of ω. For the dashed lines the conducting component has $\sigma = 3 \times 10^{-5}$ $(\Omega - \mathrm{m})^{-1}$ and the insulating component $\sigma = 3 \times 10^{-8}$ $(\Omega - \mathrm{m})^{-1}$. For the solid lines the conducting component has $\sigma = 30$ $(\Omega - \mathrm{m})^{-1}$ and the insulating component $\sigma = 3 \times 10^{-14}$ $(\Omega - \mathrm{m})^{-1}$. $\varepsilon_o \varepsilon_r = 3 \times 10^{-11}$ (Farad/m) for all components.

system shows percolation type dispersion between $\omega = 1$ and 10^9, with the properties of the components only showing up above and below these frequencies. At $\phi = 2/3$ the sample shows a frequency independent conductivity, as required by percolation theory for this highly conducting sample, up until additional dispersion, due to the conductivity, component itself sets in at $\omega = 10^{10}$. For $\phi = 0.2$ the expected slope of 2 (standard percolation theory) or $(t+1)/t = 2$ (GEM eq.) is observed only between $\omega = 10^4$ and 10^8, as the percolation behavior is limited by the properties of the components outside of this range. As indicated earlier the results shown in Figs. 12 and 13, although reasonably logical are by no means definitive and a considerable amount of work, both theoretical and experimental, remains to be done on real continuum percolation systems.

VIII. Conclusions

A considerable amount of theoretical and experimental work remains to be done in order to find out to what extent some or all of the ideas, models and equations given in this paper can be used in practice.

References

1. R. Landauer, in *Electrical Transport and Optical Properties of Inhomogeneous Media,* edited by J.C. Garland and D.B. Tanner (AIP Conf. Proc. 40, New York, 1978), pp. 2–45.
2. D.S. McLachlan, M. Blaszkiewics, and R.E. Newnham, *J. Am. Ceram. Soc*., **73**, 2187 (1990).
3. D. Stauffer and A. Ahorony, *Introduction to Percolation Theory* (Taylor and Francis, London, 1994).
4. *Percolation Processes and Structures*, edited by G. Deutscher, R. Zallen and J. Adler (Annals of the Israeli Physical Society, Vol. 5, Jerusalem, 1983).
5. D.J. Bergman and D. Stroud, in *Solid State Physics,* **46** (Academic Press, San Diego, 1992), p. 147.
6. Ce-Wen Nan, *Prog. in Mat. Sci*., **37**, 1 (1993).
7. J.P. Clerc, G. Girand, J.M. Langier, and J.M. Luck, *Adv. Phys*., **39**, 191 (1990).
8. R.E. Meredith and C.W. Tobias, in *Advances in Electrochemistry and Electrochemical Engineering,* Vol. 2, edited by C.W. Tobias (Interscience, New York, 1962), p. 15.
9. R. Zallen, *The Physics of Amorphous Solids* (John Wiley, New York; 1983), ch. 4.
10. D.S. McLachlan, *Electrically Based Microstructure Characterization* Materials Research Society Symposium Proceedings, Vol. 411, 309 (1996).
11. S.N. Roberts and L.M. Schwartz, *Phys. Rev*., **B31**, 5990 (1985).
12. R.P. Kusy, *J. Appl. Phys*., **48**, 5301 (1977).
13. I. Balberg, *Phil. Mag*., **B56**, 991 (1987); *Phys. Rev. Lett*., **59**, 1305 (1987).
14. F. Carmona, P. Prudhon, and F. Baweau, *Solid St. Comm*., **51**, 255 (1984).
15. Junjie Wu and D.S. McLachlan, *Phys. Rev*., **B56**, 1236 (1997).
16. Junjie Wu and D.S. McLachlan, *Phys. Rev*., **B58**, 14880 (1998).
17. D.S. McLachlan, W.D. Heiss, C. Chiteme, and Junjie Wu, *Phys. Rev*., **B58**, 13558 (1998).
18. D.S. McLachlan, *Physica*, **B254**, 249 (1998).
19. C. Chiteme and D.S. McLachlan, *Electrically Based Microstructure Characterization II*, Materials Research Society Symposium Proceedings. **500**, 357 (1988) and private communications.
20. D.S. McLachlan, J.-H. Hwang, and T.O. Mason, *J. Electroceramics*, **5**, 37 (2000).
21. D.S. McLachlan, R. Rosenbaum, A. Albers, G. Eytan, N. Grammatika, G. Hurwitz, J. Pickup, and E. Zalen, *J Phys.: Condensed Matter*, **5**, 4829 (1993).
22. G Eytan, R. Rosenbaum, D.S. McLachlan, and A. Albers, *Physical Review B*, **48**, 6342 (1993).
23. J. Shoskany, V. Goldner, R. Rosenbaum, M. Witcomb, D.S. McLachlan, A. Pakervski, A. Gladishi, and Y. Lereah, *J Phys.: Condensed Matter*, **8**, 1729 (1996).
24. K.S. Cole and R.H. Cole, *J. Chem. Phys*., **9**, 341 (1941).
25. S. Harviliak Jr, and S. Neganu, *J. Polymer Science, Pt C*, **14**, 99 (1966).